JOIV : Int. J. Inform. Visualization, 7(3-2): Empowering the Future: The Role of Information Technology in Building Resilience - November 2023 1022-1031

INTERNATIONAL JOURNAL ON INFORMATICS VISUALIZATION

journal homepage : www.joiv.org/index.php/joiv

Mobile Implementation of Retinal Image Analysis for Efficient Vessel, Optic Disc, and Lesion Detection

Mubdiul Hossain [a], Aziah Ali [a,*], Noramiza Hashim [a], Wan Noorshahida Mohd Isa [a], Wan Mimi Diyana Wan Zaki [b], Aini Hussain [b]

[a] *Faculty of Computing & Informatics, Multimedia University, Selangor, Malaysia*
[b] *Faculty of Engineering & Built Environment, Universiti Kebangsaan Malaysia, Selangor, Malaysia*
*Corresponding author: *aziah.ali@ieee.org*

Abstract*— Smartphone-based mobile fundus photography is gaining popularity due to the rise of handheld fundus lenses, allowing a portable solution for a mobile-based computer-assisted diagnostic system (CADS). With such a system, professionals can monitor and diagnose numerous retinal diseases, including diabetic retinopathy (DR), glaucoma, age-related macular degeneration, etc. on their smartphone devices. In this study, we proposed a unified CADS tool for smartphone devices that can detect and identify six crucial retinal features utilizing both a filtering approach and a deep learning (DL) approach. These features are retinal blood vessels (RBV), optic discs (OD), hemorrhages (HM), microaneurysm (MA), hard exudates (HE), and soft exudates (SE). Traditional filtering is applied for RBV segmentation using B-COSFIRE and Frangi filter, whereas vessel inpainting and automatic canny edge-based Hough transform are used to localize OD center and radius. The DR lesions (HM, MA, HE, OD segmentation, and SE) are detected using a transfer learning-based Resnet50 backbone and multiclass DL U-net architecture. RBV segmentation achieved 94.94% and 94.44% accuracy in the DRIVE and STARE datasets. OD localization achieved an accuracy of 99.60% in the MESSIDOR dataset. Lastly, the IDRiD dataset is used to train and validate the DR lesions with an overall accuracy of 99.7%, F1-score of 77.4, and mean IoU of 59.2. The smartphone application can perform all the segmentation tasks at once in an average of 30 seconds. Given the availability, it is possible to improve the accuracy of the DL method further by training with more mobile fundus datasets.

***Keywords*— Mobile application; retinal image analysis; fundus image; diabetic retinopathy; lesion detection; vessel segmentation; optic disc localization**

Manuscript received 18 Dec. 2022; revised 29 Jun. 2023; accepted 12 Aug. 2023. Date of publication 30 Nov. 2023.

I. INTRODUCTION

Retinal fundus cameras are modern-day medical imaging devices used to capture the inner surface of the eye, i.e., the retina. The captured images are called retinal fundus images containing important landmarks of the retina such as retinal blood vessels (RBV), optic discs (OD), macula, fovea, retinal background, etc. Ophthalmologists use these captured fundus images and diagnose the landmarks by identifying potential symptoms that may indicate health risks [1]. These images may show signs of lesions such as hemorrhages, microaneurysm, exudates, neovascularization, retinal tearing, optic cup formation, vessel caliber, tortuosity, etc. Depending on each symptom's severity, diabetic retinopathy (DR), retinal detachment, glaucoma, hypertension, diabetes, kidney dysfunction, age-related macular degeneration (AMD), and other ocular and systemic diseases can be diagnosed and treated by professionals [2]–[7]. Therefore, it is a crucial diagnostic tool for both medical professionals and patients for early detection of these diseases to prevent partial or complete blindness.

To properly diagnose the fundus images, expert physicians examine the retinal structures by manually segmenting the retinal blood vessels (RBV), OD localization and segmentation, lesions identification, and grading. It is a tedious and time-consuming process for the experts, especially when the quantity of the image increases, thus leading researchers to an easier solution, such as computer-aided diagnostic system (CADS) tools. Nowadays, various CADS tools are proposed by the researchers, such as RBV segmentation CADS tools are used to find abnormalities by calculating the retinal vascular network to indicate potential signs such as vessel tortuosity and leakage [8]. Like RBV CADS tools, OD localization and segmentation CADS are proposed to help diagnose glaucoma [9]. Recent advancements in machine learning (ML) and deep learning (DL) techniques opened the door for more accurate results as well as an automatic screening of DR while lowering the cost and increasing patients' access to DR screening [10].

Although traditional desktop fundus (DF) cameras capture high-quality images, they are very expensive and require additional setup, which hinders accessibility in resource-limited settings and lacks portability. A handheld fundus (HF) lens is an alternative to DF cameras, which work similarly to an ophthalmoscope. A device with a camera, such as a smartphone, is attached to the lens that can capture the image of the retina [11]. These lenses are already commercially available, making it possible to utilize a smartphone-based CADS for a cheaper, portable diagnosis alternative that can benefit in a limited resource environment.

A. Retinal Blood Vessel Segmentation

Various researchers have conducted many RBV segmentation studies over the past few decades. As time progressed, RBV segmentation techniques shifted from the traditional filtering approach to deep learning techniques. Traditional filtering approaches are categorized into five sections, i.e., pattern classification, morphological processing, vessel tracking, matched filtering, and multiscale approaches [12]. Though these approaches are considered earlier methods, they are still being investigated in recent years.

Bar Combination of Shifted Filter Responses (B-COSFIRE) is a traditional bio-inspired filter based on key-point detection and pattern recognition [13], [14]. The original author achieved 94.42% and 94.97% accuracy in Digital Retinal Images for Vessel Extraction (DRIVE) and Structured Analysis of the Retina (STARE) databases, respectively. This filter's accuracy was improved in a few recent studies, e.g., by applying the multiscale Frangi filter and Otsu's thresholding [15], optimal parameter optimization [16], and adaptive thresholding with automatic parameter estimation [17].

Other notable methodologies were also conducted based on unsupervised traditional approaches. They are Soares et al.'s approach using 2-D Gabor wavelet [18], Gaussian Matched filter introduced by Chaudhuri et al. [19], Matched filter response with adaptive thresholding by Hoover et al. [20]. Later, a few other researchers incorporated supervised classification methods by classifying fundus image pixels as vessel pixels or non-vessel pixels with the traditional methods [21]–[23].

The key difference between supervised and unsupervised classification is that supervised algorithms extract vessels based on training ground truth data, and unsupervised methods find inherent patterns within the image to be categorized as blood vessels or non-blood vessel pixels [12]. Because of that, unsupervised methods are usually less computationally expensive and do not rely on a large amount of ground truth data but are less accurate than supervised methods. However, the supervised classifier's requirement for ground truth data also plays a key role in achieving higher accuracy, which can result in lower accuracy when ground truth data is insufficient.

Most techniques discussed above also apply some pre-processing steps such as green channel image (GCI) extraction, contrast limited adaptive histogram equalization (CLAHE), gaussian filter, etc. Post-processing steps such as morphological closing, opening, and thresholding are also applied to improve vessel detection rate.

The evolution of the DL method in modern times allowed for improved accuracy in terms of sensitivity and specificity. A DL architecture consists of several hierarchical layers and an encoder and decoder that extract higher-level features from the input [24]. Depending on the layer type, quantity, and depth, numerous architectures such as convolutional neural network (CNN), multiscale CNN, fully convolutional neural network (FCN), recurrent neural networks (RNN), deep neural network (DNN), and artificial neural network (ANN) has been proposed that were applied for RBV segmentation [25], [26].

Among these, CNN is widely used to classify and segment RBV. It is constructed with three main layers: convolutional, pooling, and fully connected. AlexNet, Inception-v3, and Resnet are a few of the pre-trained CNN architectures used to classify RBV. Fan & Mo, Liskowski & Krawiec, and Uysal & Güraksin proposed RBV segmentation studies with CNN that achieved an accuracy of 96.12%, 94.95%, and 94.19% in DRIVE and 96.14%, 95.66%, and 94.71 in STARE datasets which are higher compared to many previous traditional filtering approaches [27]–[29].

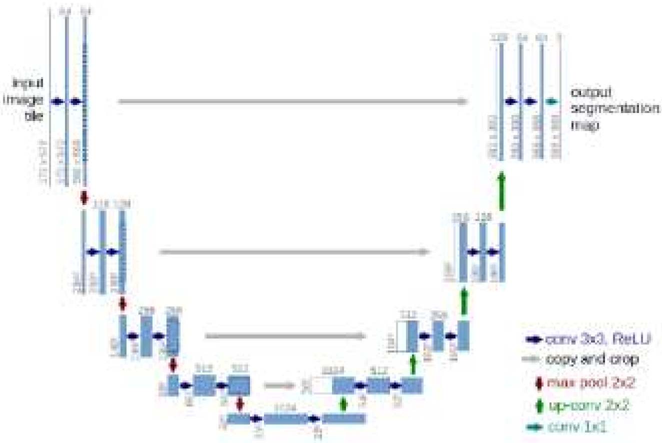

Fig. 1 U-net Architecture [30].

Out of the many DL architectures mentioned, U-net architecture [30] has been explored the most by many researchers to address several aspects of vessel detection shortcomings to improve accuracy over the previous networks. Its structure consists of symmetrical encoders and decoders, which form a shape like "U" hence the name (Fig. 1). A full comprehensive recent result of multiple studies for U-net architecture is discussed by [26].

B. Optic Disc Localization and Segmentation

Researchers have been investigating the OD part of the fundus image to help medical professionals perform retinal image analysis more accurately and efficiently. A dependable technique for segmenting the optic disc is crucial in establishing a point of reference for identifying optic nerve head disorders such as glaucoma and DR [9]. This is essential for the automated screening of abnormalities in the optic nerve head. There are two different methods in the OD analysis research area. The OD localization method detects the OD center and radius; the other is the OD segmentation to identify every pixel belonging to the whole OD.

The OD region has a higher contrast against the retinal background, making it easy to spot. Past techniques utilized thresholding [31], [32], contrast-based [33], [34], vessel inpainting [35], Hough transform [36]–[38] and morphological algorithm [39] methods to segment or localize OD. DL methods have also been studied for automatic OD segmentation. Similar to the RBV methodologies DL method, corresponding segmented OD ground truth is also required to train a DL model. Few databases, such as MESSIDOR [40], Drishti-GS [41], Indian Diabetic Retinopathy Image Dataset (IDRiD) [42] provide ground truth data. A lot of the same DL architectures, as discussed in section II (A) are also employed in OD detection using CNN, FCN, U-net, etc. According to a recent study [43], U-net and generative adversarial network (GAN) models have shown impressive results for OD segmentation as well as glaucoma detection.

C. Diabetic Retinopathy Screening

DR is an ocular complication of diabetes that leads to swelling and leakage of fluids and blood from blood vessels in the retina. These leakages are forms of lesions, namely, microaneurysms (MA), hemorrhages (HM), and soft and hard exudates (EX) [44]. Depending on the presence of these lesions, DR is categorized into five stages based on a severity scale starting from no DR, mild non-proliferative DR (NPDR), moderate NPDR, severe NPDR, and proliferative DR(PDR) [45]. DR lesion detection and DR classification are the most common methodologies in DR-CADS where detection is done by segmentation to visualize the lesions, and classification is to grade the severity scale of DR.

According to Alyoubi et al. [44], DR classifications are divided into four categories, namely binary, multi-level, lesion-based, and vessel-based classification. In binary classification, DR is classified into two classes that are normal images (no DR) and DR images [46]–[48]. Multi-level classifications are divided into many classes ranging from three to five stages of DR [49]–[53]. Lesion-based studies involved detecting specific lesions such as MA [54], HM [55], or EX [56], [57].

Most of these methods use DL approaches to classify based on various versions of CNN and FCN architecture with basic data augmentation to increase dataset size and use pre-trained networks. While most research performed the segmentation of different lesions separately, few have proposed a multi-class semantic segmentation model to extract features [58], [59]. MESSIDOR, IDRiD, DIARETDB1 [60], DDR [61] are the most commonly used databases in these studies that provide grading or pixel-level ground truth data.

D. Mobile-based Retinal Analysis Methods

Several smartphone-based fundus imaging devices, such as 20D lens, D-Eye, Peek Retina, iExaminer, and iNview [62] are readily available, similar to Fig. 2(a). They are HF lenses that can be attached to a smartphone device to capture various ranges of mobile fundus images (Fig. 2b). Usually, these lenses produce a very narrow field of view (FOV) and low-resolution image compared to DF cameras, but they are portable, compact, and cheaper solutions [63]. Another drawback of the HF lens is it requires some adjusting before capturing a usable fundus image to avoid glaring and incorrect focal distance.

The smartphone device is crucial in capturing the actual fundus image through the HF lens. Smartphone devices have come a long way both in photography and computational power. Nowadays, an average smartphone camera can capture high-resolution images with high dynamic range and can process ML and DL algorithms locally on the device [65]. This opens the possibility of not only processing HF-produced fundus images but also DF-produced images on the smartphone device as well.

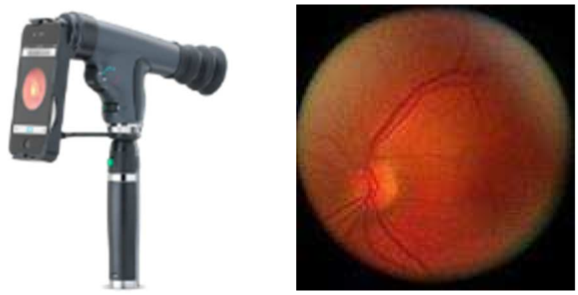

(a) (b)

Fig. 2 (a) A handheld fundus lens attached to a smartphone [62], (b) Mobile Fundus Image [64].

With its availability, few researchers have been investigating smartphone-based CADS that can perform multiple retinal analysis tasks. Xu et al. proposed an RBV segmentation using the traditional filtering approach using the Gabor filter and bottom-hat transformation [66]. Previously, a smartphone-based RBV segmentation method using an optimized B-COSFIRE filter was investigated for Android devices [67] that achieved comparable performance to the desktop implementations. Khaing et al. proposed an OD segmentation method on smartphone-captured fundus images by extracting vessel structures[68].

While others also attempted DR detection methodologies using DL techniques on smartphone devices [11], [69]–[71]. It is important to note that most of the DR screening study for mobile implementation focuses only on the HF lenses and the application. The core methodologies they used for DR screening are various off-the-shelf Artificial Intelligence (AI) and DL-based software available on the market.

TABLE I
PREVIOUS STUDIES ON SMARTPHONE-BASED FUNDUS ANALYSIS METHODS. S = SEGMENTATION, G = GRADING

Author	RBV	OD	DR	Method	S/G	Result
Xu et al. [66]	Yes	No	No	Filter based	S	Accuracy = 92.65%
Rajalakshmi et al. [71]	No	No	Yes	AI-based	G	Sensitivity = 95.80% Specificity = 80.20%
Hacisoftaoglu et al. [69]	No	No	Yes	DL based	S	Accuracy = 98.60%
Hossain et al. [67]	Yes	No	No	Filter based	S	Accuracy = 95.42%
Khaing et al. [68]	No	Yes	No	Filter based	S	Precision = 92.64%

Table 1 summarizes a number of published studies on smartphone-based fundus image analysis methods. Few authors have approached different solutions in specific domains to introduce this analysis approach using HF lenses. However, smartphone CADS are not globally popularized yet due to the lack of studies, as no CADS can perform multiple feature extraction analyses simultaneously from mobile fundus images. A unified approach of multiple-feature extraction is appropriate for a better retinal image analysis system by analyzing the DR lesions and other crucial retinal features that may indicate DR symptoms, opening the door to multi-feature smartphone-based retinal image screening.

In this study, we approached a unified RBV, OD, and DR lesion segmentation method in a smartphone application that addresses the gaps mentioned in the research fields. Due to the vast size of this domain, the scope of this study is limited to segmentation only. Classification of disease/grading is a potential field that may be investigated further.

II. Materials and Method

The overall methods are divided into two sections: the filtering approach and the deep learning approach. RBV segmentation and OD localization are performed using traditional filtering, whereas the DL method is used for lesion detection. Fig. 3 shows the overview of the proposed solution. The retinal image is loaded or captured in the Android ecosystem, and the actual image processing is executed in a Python software development kit (SDK) within the Android ecosystem. Fundus image is resized and encoded into byte array and then passed to the python SDK, decoded as a red, green, and blue (RGB) image for processing. After this step, each feature extraction method is followed and discussed in the following sections.

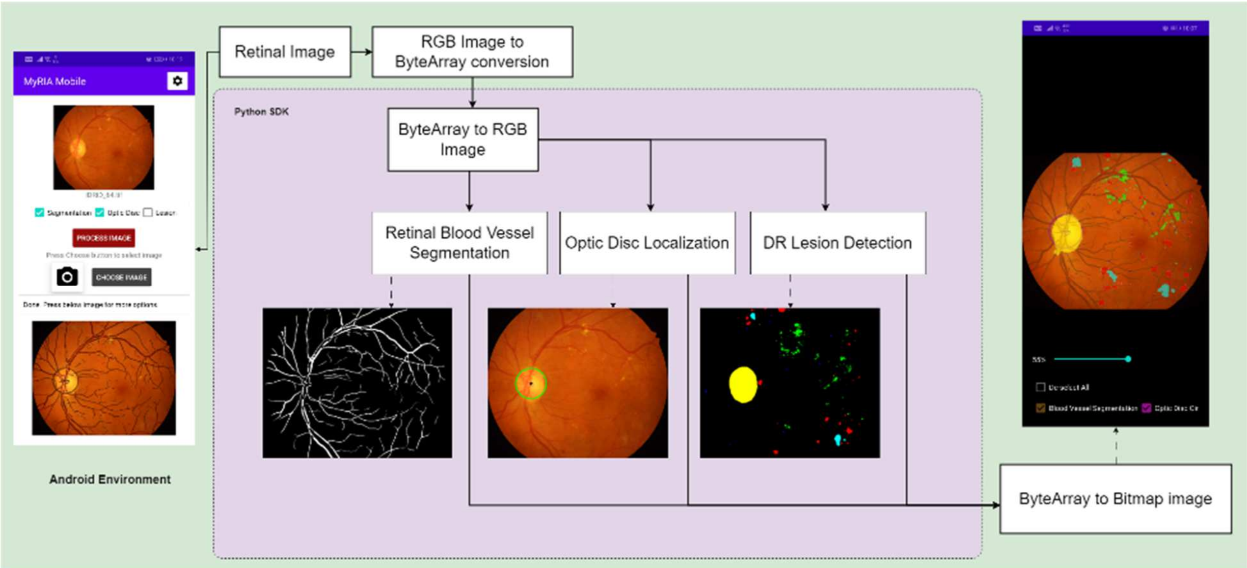

Fig. 3 Overview of the proposed mobile implementation of RBV Segmentation, OD Localization, and DR Lesion Detection.

A. Retinal Blood Vessel Segmentation

The RBV segmentation method is an extended study of a previous approach conducted by our previous work [67]. The key difference is including the Frangi filter and fine-tuning the parameters. Fig. 4 illustrates the framework overview of RBV segmentation.

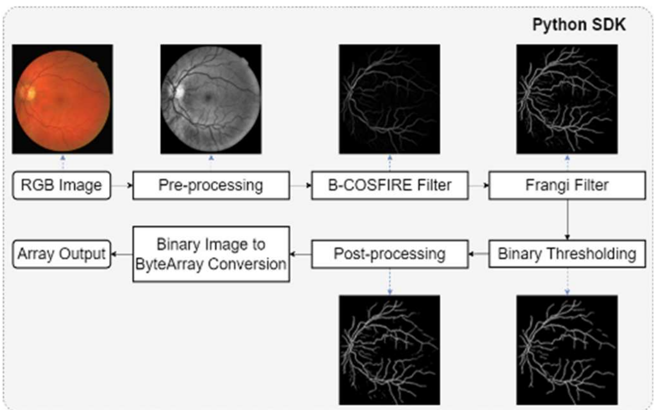

Fig. 4 RBV segmentation overview

The first step is pre-processing by extracting the green channel image (GCI) from the RGB image, identifying, and padding the region of interest (ROI) for generating a corresponding mask that identifies the field of view (FOV). GCI is extracted because the green channel has the highest contrast against the retinal background. CLAHE filter with clip limit parameter 0.015 is applied to the GCI to enhance the contrast for better blood vessel detection.

Next, the Python implementation of the B-COSFIRE filter is used to extract a grayscale image of the vessels. The B-COSFIRE filter requires two types of parameters, i.e., symmetric and asymmetric filter parameters. The original parameter from Azzopardi et al. is also used in this method [13]. The B-COSFIRE grayscale output is inverted and passed as a Frangi filter input to highlight finer vessels, producing a grayscale image. The sigma parameters from the B-COSFIRE filter were also applied to Frangi filter.

This Frangi grayscale output is binarized with ISODATA thresholding. The binary image usually contains some noise and gaps within the vessels, which are removed using morphological closing and opening. The binarized vessel output is converted to byte arrays and is passed to the graphical user interface (GUI).

B. Optic Disc Localization

For OD localization, the retinal RGB image also goes through pre-processing step, where the red and blue (RB) channel is extracted and combined. Concurrently, the RGB image is converted into CIELab format, and the L* channel is extracted for ROI masking. Then, the ROI of the RB image is extended by padding around the edge of the image boundary using the mask. This padded image is copied into two, and the CLAHE method is applied to one of them to extract blood vessels.

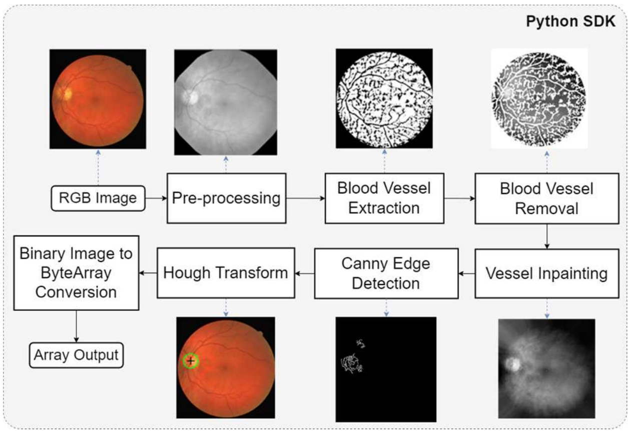

Fig. 5 OD Localization overview

Extraction of the vessels is conducted by background subtraction using a convolve 2D filter on the CLAHE image. Otsu's method is applied to binarize the background subtracted image. The binarized image is inverted and multiplied with the other padded image so that all the black pixels are set to null values. These null values are replaced with the neighboring values during the inpainting method in a certain way so that instead of the vessels, a uniform distribution of the background pixel is formed, thus replacing the vessels with the retinal background.

An automatic canny edge parameter method is proposed by applying Gaussian blur on the in-painted image. Then, the median value of the blurred image is taken and multiplied with a positive and negative sigma value of 0.8. This automatically generates a lower and upper parameter value that is passed as Hough Transform parameter 2 and parameter 1. The Hough Transform outputs OD center and radius coordinates if a circle is detected and later visualized by drawing the circle on the original RGB image and is passed to the GUI (Fig. 5).

C. Diabetic Retinopathy Lesion Detection

Using a transfer learning approach, we proposed a multi-class semantic segmentation DL method to detect DR lesions. Resnet50 is used as the backbone pre-trained network, and U-net is used as the decoder (Fig. 6). The Resnet50 encoder employs the pre-trained weights by ImageNet Large Scale Visual Recognition Challenge 2012 (ILSVRC2012) with 1,000,000 labeled images [72], and the U-net architecture utilizes the various features classified by the pre-trained network to predict segmentation outputs [73].

IDRiD dataset provides five different classes of ground truth segmentation for 84 digital fundus images, namely, hemorrhages (HM), microaneurysms (MA), hard exudates (HE), soft exudates (SE), and optic disc (OD). Among these, all except OD are classed as DR lesions. However, OD may indicate potential signs of DR based on its size and formation. Also, not all 84 images have an equal distribution of ground truth masks for all classes.

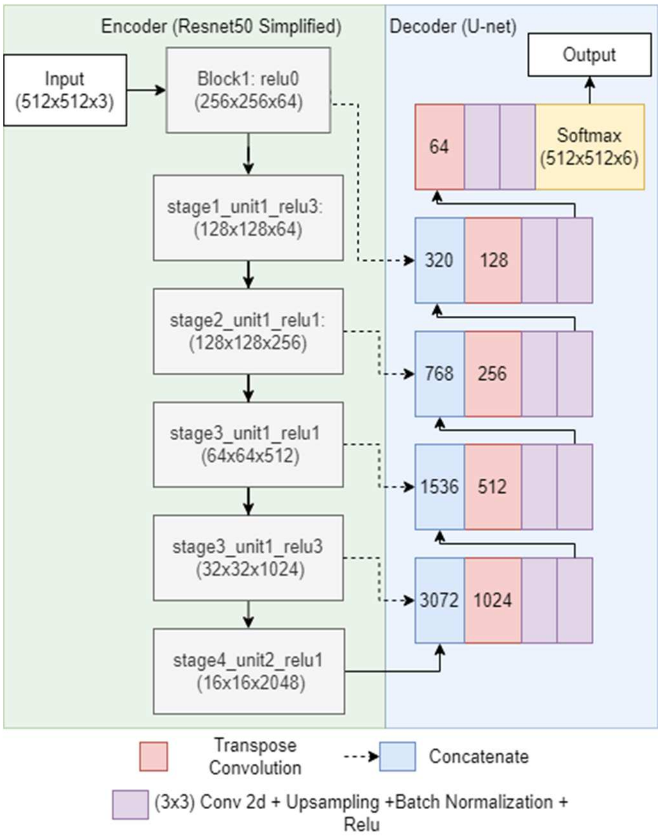

Fig. 6 Combined Resnet50 and U-net model [73].

The non-ROI, i.e., the black regions, are removed by identifying the retinal background and converting the RGB image to CIELab format image. The L* channel from this image is selected, and ISODATA is applied to create a mask that represents the ROI. Then, using the Canny edge detection method, the ROI top, bottom, left, and right areas are identified and cropped from the original RGB image, as shown in Figure 7(a). The removed non-ROI are the unnecessary black regions that do not contain any meaningful information, thus improving learning during training. On the other hand, ground truth masks are also cropped according to their corresponding cropped RGB image size.

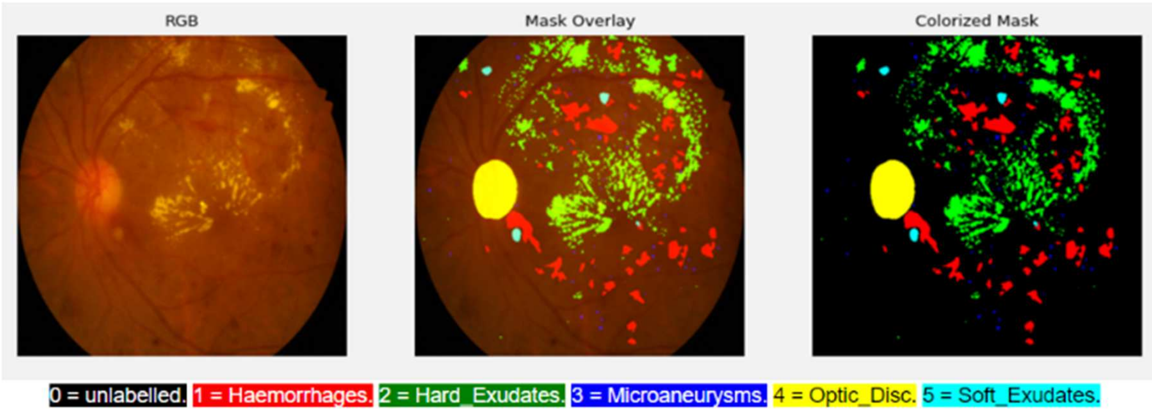

Fig. 7 (a) ROI cropped image (left), (b) Mask overlay (middle), (c) colorized mask label (right).

Each ground truth mask contains two-pixel values: lesion pixels (white) or non-lesion pixels (black). As there are multiple classes of ground truth masks for a single RGB, all the mask images are converted into one label mask for multiclass classification. This label mask contains values ranging from 0-5 that represent each class as illustrated in Fig. 7(c). All the images are resized into 512x512 resolution for training.

The IDRiD dataset does not have an equal number of segmentation ground truth masks for every class resulting in an imbalance problem. Therefore, data augmentation such as cropping, shear, zoom, flip, normalization, etc. is applied to increase the dataset size to reduce the imbalance issue. The dataset is divided into 54 training sets and 27 validation sets. During training, each label mask image is converted into a one-hot encoded image with a size of 512x512x6. The training configuration consists of batch size 4, Adam optimizer with learning rate 0.0001, Softmax activation with 6 classes as the last dense layer, 15 epochs, and Dice coefficient, and categorical focal loss is used as the loss function. The loss L is as follows:

$$L = \frac{(1+\beta^2)\times tp}{(1+\beta^2)\times fp + \beta^2 \times fn + fp} + (-gt \times log(pr) - (1-gt)\times log(1-pr)) \quad (1)$$

Where tp = true positive, fp = false positive, fn = false negative, gt = ground truth, pr = prediction, and β = 1. Intersection over union (IOU) and F1 score are monitored during model training.

The model outputs prediction as a 512x512x6 shape where each array of the last depth represents a single lesion class. Every pixel in each class is a probability value that corresponds to its dimension. The higher the probability value, the more likely that pixel of that class is detected as a lesion. Since this is a multi-class approach, each pixel is mutually exclusive. That is why a label mask is generated where each pixel is the class indices of the prediction that has the highest probability for that pixel location. This label mask can be converted into a one-hot encoded image for extracting binary segmentation mask for each class or can be visualized by color coding the labels. The Resnet50+U-Net model was trained on the Google Cloud Platform on a GPU with 12GB of VRAM due to a large number of augmented images.

III. Results and Discussions

Quantitative and qualitative assessment for this study is divided into three sections to distinguish each aspect of segmentation methods. Since all the methods are based on segmentation outputs, the key metrics for quantitative assessment are the same for all the extracted features and summarized in Table II, where TP = true positive – indicates correctly identified white pixels (Ones), TN = true negative – correctly identified black pixels (Zeros), FP = false positive – number of wrongly detected white pixels, and FN = false negative – wrongly detected black pixels.

Accuracy (Acc), Sensitivity (Sn), and Specificity (Sp) are measured for all the retinal segmentation outputs as these are the most commonly used metrics in previous studies. IoU and F1-score are also calculated for DR lesions segmentation outputs for each class.

TABLE II
Performance Metric for Segmentation Outputs

Metric	Definition
Sensitivity (*Sn*)	TP/(TP+FN)
Specificity (*Sp*)	TN/(TN+FP)
Accuracy (*Acc*)	(TP+TN)/(TP+TN+FP+FN)
F1-score	2TP/(2TP+FP+FN)
Intersection over Union (*IoU*)	TP/(TP+FP+FN)

The robustness of this study is performing multiple retinal segmentation tasks within low-powered settings e.g., smartphone devices. Although few mobile-based fundus datasets are available, none provide any manually annotated data that can be used for validation. Hence, a qualitative assessment is opted for the mobile fundus image dataset provided by the oDocs montaging dataset [64]. DRIVE and STARE datasets are chosen for RBV segmentation evaluation with 20 test images each. 1200 images from the MESSIDOR dataset are validated for OD localization. As for DR detection, each class i.e., HM, MA, HE, SE, and OD, containing 27 test ground truth segmentation data in the IDRiD dataset are also evaluated.

In Table III quantitative results of all the extracted features are tabulated for their respective datasets. RBV and OD results show comparable performance with the state-of-the-art methods. Specifically, for RBV segmentation, the overall accuracy and sensitivity are higher than in the previous studies as shown in Table IV. However, for DR detection, one feature i.e., MA scored considerably low due to the fact this type of lesion is exceedingly small and can be hard to detect.

TABLE III
SEGMENTATION RESULTS FOR ALL FEATURES

Features	Dataset	*Performance Metrics*					
		Sn	Sp	Acc	F1-Score	IoU	Time (seconds)
Blood Vessel	DRIVE	78.32	96.51	94.94	72.76	-	~10
	STARE	79.57	95.66	94.44	70.14	-	
Optic Disc Loc.	MESSIDOR	78.82	99.77	99.60	-	-	~5
DR (Overall)	IDRiD	74.30	99.82	99.70	77.40	59.20	~10
Haemorrhages		52.22	99.65	99.03	58.64	40.25	
Hard Exudates		64.68	99.70	99.27	68.73	55.38	
Microaneurysms		25.03	99.93	99.83	27.30	16.75	
Optic Disc Seg		96.70	99.86	99.80	95.26	91.70	
Soft Exudates		69.00	99.94	99.87	70.70	53.05	

TABLE IV
COMPARISON OF RBV SEGMENTATION RESULTS FROM THE PAST STUDIES

Method	Segmentation Performance			
	Dataset	Sn (%)	Sp(%)	Acc (%)
Proposed Method (~10 seconds)	DRIVE	78.32	96.51	94.94
	STARE	79.57	95.66	94.44
Hossain et al. [67] (~9 seconds)	DRIVE	76.12	96.65	94.87
	STARE	74.39	97.74	95.96
Azzopardi et al. [13] (~10 seconds)	DRIVE	76.55	97.04	94.42
	STARE	77.16	97.01	94.97
Xu et al. [66] (~2 minutes)	DRIVE	78.60	95.50	93.30
	STARE	82.50	93.10	92.00

While other studies have achieved higher accuracy by training the MA separately, this defeats the purpose of our scope, which is executing the model within smartphone devices. Training a model for each class will create their weights that cumulatively increase the total size of weights. Multiclass segmentation solves this issue by predicting all the classes with singular weight. On the other hand, the DL method has the best detection for OD because of its bright regions against the retinal background. Although not directly indicating a DR lesion, DL OD detection serves as a useful backup to extract OD if localization fails as well as help identify abnormal formation of the OD, which may be related to DR. Compared to a previous study by Furtado, the proposed DL method scored significantly higher IoUs for HA, MA, SE, and OD features [58].

A visual assessment can be observed in Fig. 8, where a DRIVE and mobile fundus images are processed with the proposed RBV and OD localization method. As shown in the bottom section, the proposed method can segment the retinal vessel but contains noise as the mobile fundus images are generally grainy. The OD is also successfully localized, and a circle is drawn over the fundus image where the OD is located. The qualitative study shows that the RBV method can extract most of the vessels but starts to produce noisy pixels as the vessels get smaller. This is a challenge that is very difficult to solve with traditional filtering approaches.

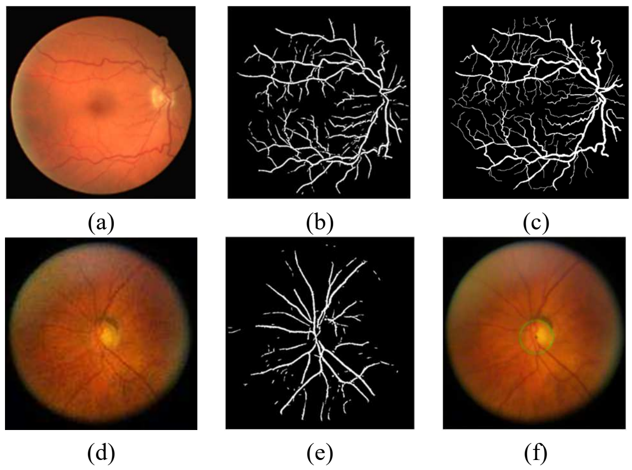

Fig. 8 (a) A DRIVE retinal fundus image, (b) Proposed RBV segmentation output, (c) Ground truth image, (d) Mobile fundus image, (e) Mobile RBV segmentation output, (f) OD localization.

Fig. 9 displays an example of a fundus image input, its respective DR prediction, and the ground truth mask. Each color of the prediction image and ground truth image represents a specific lesion type class, as illustrated and labeled in Fig. 7c. The bottom two rows are the segmented mask images extracted from the prediction output image. The visual assessment shows the prediction output image demonstrates striking resemblances with the ground truth image. These lesion data can be utilized to estimate the severity of DR by calculating the quantity of each lesion.

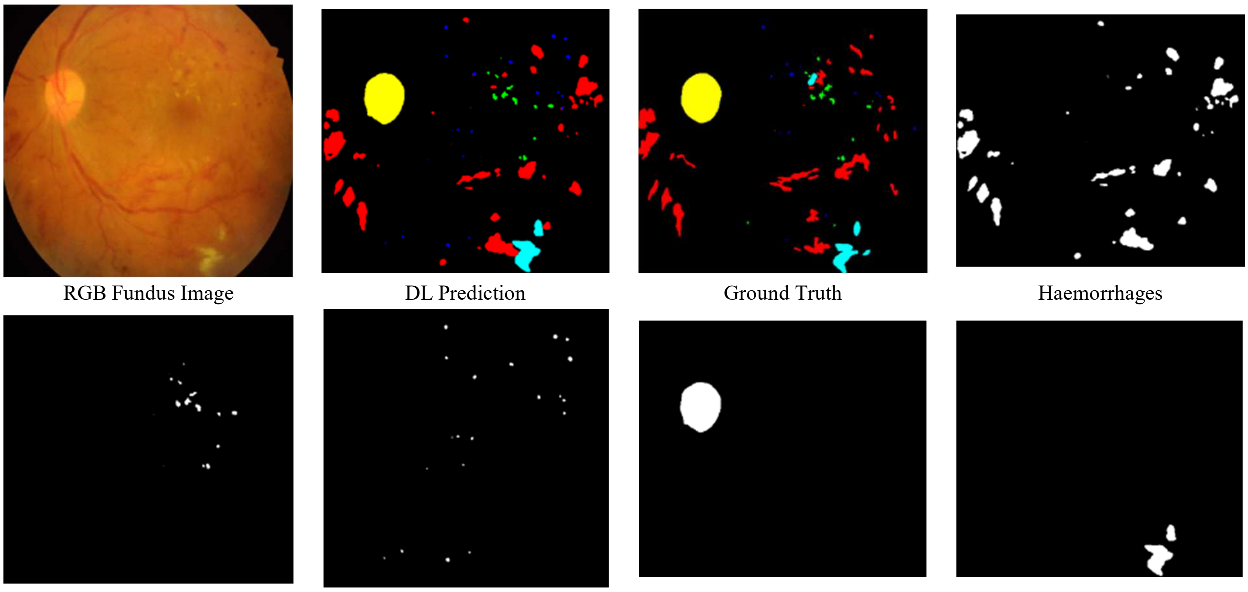

Fig. 9 DR lesion prediction and segmentation output of proposed DL model.

As proof of concept, an Android-based mobile application (Fig. 10), Mobile Retinal Image Analysis (mRIA), is developed to perform all the feature extraction mentioned in this study. The GUI is based on the Android native framework and the core backend image and DL processing is executed in a Python environment that runs within the Android ecosystem. Thus, internet accessibility is not required. Fundus images can be either captured from the mobile camera or loaded from the storage device as input.

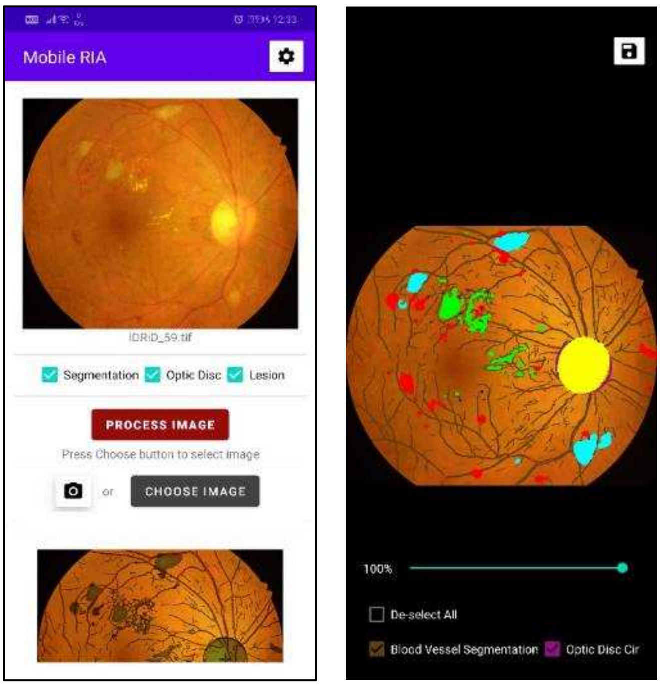

Fig. 10 Smartphone implementation of the proposed Retinal Image Analysis system.

The user can choose all or any of the three methods of segmenting features, i.e., RBV segmentation, OD, and Lesion to perform the analysis. The processed output mask images are shown in a unified image viewer (Fig. 10, right) where each mask image is color-coded to represent a specific feature and overlayed on top of the original fundus image. The user can control the opacity of the features as well as hide or show individual features.

The image and DL processing execution are done on a separate backend thread, thus making it faster to segment fundus images. On average, it takes around 25-30 seconds to process a single image to extract all six features. The DL model weight size is about 281 Megabytes (MB), and the total size of the Android Package Kit (APK) executable is about 500 MB. Therefore, executing the application locally on a device without an internet connection is proper.

The user can also customize the color of the highlighted features and save the processed output. The application was tested on Android version 7.2, 9.1, and 13 on x86, x64, and arm64-v8a architecture. On average the image processing time is about 35 seconds when all the features are selected for processing.

IV. Conclusion

In this study, a total of six retinal feature extraction methods are proposed. These are retinal blood vessel segmentation, optic disc localization and segmentation, and detection of hemorrhages, microaneurysms, hard exudates, and soft exudates. Combinatorial filtering and deep learning methodologies were proposed to extract the features. A smartphone application is developed as a prototype application that can perform these retinal feature extractions with a single button press. This opened up an opportunity for a cheap and portable retinal image analysis method suitable for resource-limited settings using handheld fundus lenses. The quantitative result shows the proposed methods achieved comparable performance with the state-of-the-art methods. Filtering approaches such as vessel extraction achieved an accuracy of 94.94% in the DRIVE and 99.44% in STARE dataset, whereas optic disc localization achieved an accuracy of 99.60% in the MESSIDOR dataset. Diabetic retinopathy lesion detection using our proposed deep learning method performed an overall accuracy of 99.70%.

ACKNOWLEDGMENT

This research is funded by the Ministry of Higher Education, Malaysia. (Grant Code: FRGS/1/2020/TK0/MMU/03/15).

REFERENCES

[1] K. H. Nguyen, B. C. Patel, and P. Tadi, "Anatomy, Head and Neck: Eye Retina," *StatPearls*, Aug. 2022, Accessed: Apr. 26, 2023. [Online]. Available: https://www.ncbi.nlm.nih.gov/books/NBK542332/

[2] S. D. Candrilli, K. L. Davis, H. J. Kan, M. A. Lucero, and M. D. Rousculp, "Prevalence and the associated burden of illness of symptoms of diabetic peripheral neuropathy and diabetic retinopathy," *J Diabetes Complications*, vol. 21, no. 5, pp. 306–314, Sep. 2007, doi: 10.1016/J.JDIACOMP.2006.08.002.

[3] R. F. Gariano and C.-H. Kim, "Evaluation and Management of Suspected Retinal Detachment," *Am Fam Physician*, vol. 69, no. 7, pp. 1691–1699, Apr. 2004, Accessed: Apr. 26, 2023. [Online]. Available: https://www.aafp.org/pubs/afp/issues/2004/0401/p1691.html

[4] L. Quaranta, I. Riva, C. Gerardi, F. Oddone, I. Floriano, and A. G. P. Konstas, "Quality of Life in Glaucoma: A Review of the Literature," *Advances in Therapy 2016 33:6*, vol. 33, no. 6, pp. 959–981, Apr. 2016, doi: 10.1007/S12325-016-0333-6.

[5] M. K. Ikram, J. C. M. Witteman, J. R. Vingerling, M. M. B. Breteler, A. Hofman, and P. T. V. M. De Jong, "Retinal Vessel Diameters and Risk of Hypertension," *Hypertension*, vol. 47, no. 2, pp. 189–194, Feb. 2006, doi: 10.1161/01.HYP.0000199104.61945.33.

[6] M. B. Sasongko *et al.*, "Retinal arteriolar tortuosity is associated with retinopathy and early kidney dysfunction in type 1 diabetes," *Am J Ophthalmol*, vol. 153, no. 1, 2012, doi: 10.1016/J.AJO.2011.06.005.

[7] A. Chopdar, U. Chakravarthy, and D. Verma, "Age related macular degeneration," *BMJ*, vol. 326, no. 7387, pp. 485–488, Mar. 2003, doi: 10.1136/BMJ.326.7387.485.

[8] K. Mittal and V. M. A. Rajam, "Computerized retinal image analysis - a survey," *Multimed Tools Appl*, vol. 79, no. 31–32, pp. 22389–22421, Aug. 2020, doi: 10.1007/S11042-020-09041-Y/TABLES/7.

[9] A. Almazroa, W. Sun, S. Alodhayb, K. Raahemifar, and V. Lakshminarayanan, "Optic disc segmentation for glaucoma screening system using fundus images," *Clin Ophthalmol*, vol. 11, p. 2017, Nov. 2017, doi: 10.2147/OPTH.S140061.

[10] A. Grzybowski *et al.*, "Artificial intelligence for diabetic retinopathy screening: a review," *Eye 2019 34:3*, vol. 34, no. 3, pp. 451–460, Sep. 2019, doi: 10.1038/s41433-019-0566-0.

[11] U. Iqbal, "Smartphone fundus photography: a narrative review," *Int J Retina Vitreous*, vol. 7, no. 1, pp. 1–12, Dec. 2021, doi: 10.1186/S40942-021-00313-9/FIGURES/9.

[12] M. M. Fraz *et al.*, "Blood vessel segmentation methodologies in retinal images – A survey," *Comput Methods Programs Biomed*, vol. 108, no. 1, pp. 407–433, Oct. 2012, doi: 10.1016/J.CMPB.2012.03.009.

[13] G. Azzopardi, N. Strisciuglio, M. Vento, and N. Petkov, "Trainable COSFIRE filters for vessel delineation with application to retinal images," *Med Image Anal*, vol. 19, no. 1, pp. 46–57, Jan. 2015, doi: 10.1016/J.MEDIA.2014.08.002.

[14] N. Strisciuglio, G. Azzopardi, M. Vento, and N. Petkov, "Supervised vessel delineation in retinal fundus images with the automatic selection of B-COSFIRE filters," *Mach Vis Appl*, vol. 27, no. 8, pp. 1137–1149, Nov. 2016, doi: 10.1007/S00138-016-0781-7/TABLES/3.

[15] K. B. Khan, A. A. Khaliq, A. Jalil, and M. Shahid, "A robust technique based on VLM and Frangi filter for retinal vessel extraction and denoising," *PLoS One*, vol. 13, no. 2, p. e0192203, Feb. 2018, doi: 10.1371/Journal.PONE.0192203.

[16] S. A. Badawi and M. M. Fraz, "Optimizing the trainable B-COSFIRE filter for retinal blood vessel segmentation," *PeerJ*, vol. 6, no. 11, 2018, doi: 10.7717/PEERJ.5855.

[17] A. Ali, M. Diyana, W. Zaki, A. Hussain, W. M. Diyana, and W. Zaki, "Retinal blood vessel segmentation from retinal image using B-COSFIRE and adaptive thresholding," *Indonesian Journal of Electrical Engineering and Computer Science*, vol. 13, no. 3, pp. 1199–1207, 2019, doi: 10.11591/ijeecs.v13.i3.pp1199-1207.

[18] J. V. B. Soares, J. J. G. Leandro, R. M. Cesar, H. F. Jelinek, and M. J. Cree, "Retinal vessel segmentation using the 2-D Gabor wavelet and supervised classification," *IEEE Trans Med Imaging*, vol. 25, no. 9, pp. 1214–1222, Sep. 2006, doi: 10.1109/TMI.2006.879967.

[19] S. Chaudhuri, S. Chatterjee, N. Katz, M. Nelson, and M. Goldbaum, "Detection of blood vessels in retinal images using two-dimensional matched filters," *IEEE Trans Med Imaging*, vol. 8, no. 3, pp. 263–269, 1989, doi: 10.1109/42.34715.

[20] A. Hoover, "Locating blood vessels in retinal images by piecewise threshold probing of a matched filter response," *IEEE Trans Med Imaging*, vol. 19, no. 3, pp. 203–210, 2000, doi: 10.1109/42.845178.

[21] N. Memari, A. R. Ramli, M. I. Bin Saripan, S. Mashohor, and M. Moghbel, "Supervised retinal vessel segmentation from color fundus images based on matched filtering and AdaBoost classifier," *PLoS One*, vol. 12, no. 12, p. e0188939, Dec. 2017, doi: 10.1371/Journal.PONE.0188939.

[22] J. V. B. Soares, J. J. G. Leandro, R. M. Cesar-, H. F. Jelinek, and M. J. Cree, "Retinal Vessel Segmentation Using the 2-D Morlet Wavelet and Supervised Classification," 2006.

[23] S. Tang, T. Lin, J. Yang, J. Fan, D. Ai, and Y. Wang, "Retinal vessel segmentation using supervised classification based on multiscale vessel filtering and gabor wavelet," *J Med Imaging Health Inform*, vol. 5, no. 7, pp. 1571–1574, Nov. 2015, doi: 10.1166/JMIHI.2015.1565.

[24] L. Deng and D. Yu, "Deep Learning: Methods and Applications," *Foundations and Trends® in Signal Processing*, vol. 7, no. 3–4, pp. 197–387, 2014, doi: 10.1561/2000000039.

[25] M. Badar, M. Haris, and A. Fatima, "Application of deep learning for retinal image analysis: A review," *Comput Sci Rev*, vol. 35, p. 100203, Feb. 2020, doi: 10.1016/J.COSREV.2019.100203.

[26] C. Chen, J. H. Chuah, R. Ali, and Y. Wang, "Retinal vessel segmentation using deep learning: A review," *IEEE Access*, vol. 9, pp. 111985–112004, 2021, doi: 10.1109/ACCESS.2021.3102176.

[27] Z. Fan and J. J. Mo, "Automated blood vessel segmentation based on de-noising auto-encoder and neural network," *Proc Int Conf Mach Learn Cybern*, vol. 2, pp. 849–856, Jul. 2016, doi: 10.1109/ICMLC.2016.7872998.

[28] P. Liskowski and K. Krawiec, "Segmenting Retinal Blood Vessels with Deep Neural Networks," *IEEE Trans Med Imaging*, vol. 35, no. 11, pp. 2369–2380, Nov. 2016, doi: 10.1109/TMI.2016.2546227.

[29] E. Uysal and G. E. Güraksin, "Computer-aided retinal vessel segmentation in retinal images: convolutional neural networks," *Multimed Tools Appl*, vol. 80, no. 3, pp. 3505–3528, Sep. 2020, doi: 10.1007/S11042-020-09372-W/FIGURES/11.

[30] O. Ronneberger, P. Fischer, and T. Brox, "U-net: Convolutional networks for biomedical image segmentation," *Lecture Notes in Computer Science (including subseries Lecture Notes in Artificial Intelligence and Lecture Notes in Bioinformatics)*, vol. 9351, pp. 234–241, 2015, doi: 10.1007/978-3-319-24574-4_28.

[31] B. Karasulu, "An automatic optic disk detection and segmentation system using multi-level thresholding," *Advances in Electrical and Computer Engineering*, vol. 14, no. 2, pp. 161–172, 2014, doi: 10.4316/AECE.2014.02025.

[32] D. Marin, M. E. Gegundez-Arias, A. Suero, and J. M. Bravo, "Obtaining optic disc center and pixel region by automatic thresholding methods on morphologically processed fundus images," *Comput Methods Programs Biomed*, vol. 118, no. 2, pp. 173–185, Feb. 2015, doi: 10.1016/J.CMPB.2014.11.003.

[33] J. Dietter *et al.*, "Optic disc detection in the presence of strong technical artifacts," *Biomed Signal Process Control*, vol. 53, p. 101535, Aug. 2019, doi: 10.1016/J.BSPC.2019.04.012.

[34] J. Sigut, O. Nunez, F. Fumero, M. Gonzalez, and R. Arnay, "Contrast based circular approximation for accurate and robust optic disc segmentation in retinal images," *PeerJ*, vol. 5, no. 9, 2017, doi: 10.7717/PEERJ.3763.

[35] A. Almazroa, W. Sun, S. Alodhayb, K. Raahemifar, and V. Lakshminarayanan, "Optic disc segmentation: level set methods and blood vessels inpainting," *Medical Imaging 2017: Imaging Informatics for Healthcare, Research, and Applications*, vol. 10138, p. 1013806, Mar. 2017, doi: 10.1117/12.2254174.

[36] M. Abdullah, M. M. Fraz, and S. A. Barman, "Localization and segmentation of optic disc in retinal images using circular Hough transform and grow-cut algorithm," *PeerJ*, vol. 4, no. 5, 2016, doi: 10.7717/PEERJ.2003.

[37] Z. Fan *et al.*, "Optic Disk Detection in Fundus Image Based on Structured Learning," *IEEE J Biomed Health Inform*, vol. 22, no. 1, pp. 224–234, Jan. 2018, doi: 10.1109/JBHI.2017.2723678.

[38] A. Ali, M. Hossain, N. Hashim, W. N. M. Isa, Z. C. Embi, and S. M. Desa, "Automatic Detection of Retinal Optic Disc using Vessel Inpainting," *2022 16th International Conference on Signal-Image Technology & Internet-Based Systems (SITIS)*, pp. 254–258, Oct. 2022, doi: 10.1109/SITIS57111.2022.00028.

[39] S. Roychowdhury, D. D. Koozekanani, S. N. Kuchinka, and K. K. Parhi, "Optic disc boundary and vessel origin segmentation of fundus images," *IEEE J Biomed Health Inform*, vol. 20, no. 6, pp. 1562–1574, Nov. 2016, doi: 10.1109/JBHI.2015.2473159.

[40] E. Decencière *et al.*, "Feedback on a publicly distributed image database: The Messidor database," *Image Analysis and Stereology*, vol. 33, no. 3, pp. 231–234, 2014, doi: 10.5566/IAS.1155.

[41] J. Sivaswamy, A. Chakravarty, G. D. Joshi, and T. A. Syed, "A Comprehensive Retinal Image Dataset for the Assessment of Glaucoma from the Optic Nerve Head Analysis," 2015.

[42] P. Porwal *et al.*, "IDRiD: Diabetic Retinopathy – Segmentation and Grading Challenge," *Med Image Anal*, vol. 59, Jan. 2020, doi: 10.1016/J.MEDIA.2019.101561.

[43] M. Alawad *et al.*, "Machine Learning and Deep Learning Techniques for Optic Disc and Cup Segmentation – A Review," *Clinical Ophthalmology*, vol. 16, pp. 747–764, 2022, doi: 10.2147/OPTH.S348479.

[44] W. L. Alyoubi, W. M. Shalash, and M. F. Abulkhair, "Diabetic retinopathy detection through deep learning techniques: A review," *Inform Med Unlocked*, vol. 20, p. 100377, Jan. 2020, doi: 10.1016/J.IMU.2020.100377.

[45] C. P. Wilkinson *et al.*, "Proposed international clinical diabetic retinopathy and diabetic macular edema disease severity scales," *Ophthalmology*, vol. 110, no. 9, pp. 1677–1682, Sep. 2003, doi: 10.1016/S0161-6420(03)00475-5.

[46] M. Esfahani, M. G.-L. Electron. J., and undefined 2018, "Classification of diabetic and normal fundus images using new deep learning method," *lejpt.academicdirect.org*, Accessed: May 01, 2023. [Online]. Available: http://lejpt.academicdirect.org/A32/get_htm.php?htm=233_248

[47] G. Quellec, K. Charrière, Y. Boudi, B. Cochener, and M. Lamard, "Deep image mining for diabetic retinopathy screening," *Med Image Anal*, vol. 39, pp. 178–193, Jul. 2017, doi: 10.1016/J.MEDIA.2017.04.012.

[48] K. Xu, D. Feng, and H. Mi, "Deep Convolutional Neural Network-Based Early Automated Detection of Diabetic Retinopathy Using Fundus Image," *Molecules 2017, Vol. 22, Page 2054*, vol. 22, no. 12, p. 2054, Nov. 2017, doi: 10.3390/MOLECULES22122054.

[49] M. D. Abràmoff *et al.*, "Improved Automated Detection of Diabetic Retinopathy on a Publicly Available Dataset Through Integration of Deep Learning," *Invest Ophthalmol Vis Sci*, vol. 57, no. 13, pp. 5200–5206, Oct. 2016, doi: 10.1167/IOVS.16-19964.

[50] S. Dutta *et al.*, "Classification of Diabetic Retinopathy Images by Using Deep Learning Models Mathematical Modeling View project Predictive Analytics View project Classification of Diabetic Retinopathy Images by Using Deep Learning Models," *International Journal of Grid and Distributed Computing*, vol. 11, no. 1, pp. 89–106, 2018, doi: 10.14257/ijgdc.2018.11.1.09.

[51] V. Gulshan *et al.*, "Development and Validation of a Deep Learning Algorithm for Detection of Diabetic Retinopathy in Retinal Fundus Photographs," *JAMA*, vol. 316, no. 22, pp. 2402–2410, Dec. 2016, doi: 10.1001/JAMA.2016.17216.

[52] H. Pratt, F. Coenen, D. M. Broadbent, S. P. Harding, and Y. Zheng, "Convolutional Neural Networks for Diabetic Retinopathy," *Procedia Comput Sci*, vol. 90, pp. 200–205, Jan. 2016, doi: 10.1016/J.PROCS.2016.07.014.

[53] X. Wang, Y. Lu, Y. Wang, and W. B. Chen, "Diabetic retinopathy stage classification using convolutional neural networks," *Proceedings - 2018 IEEE 19th International Conference on Information Reuse and Integration for Data Science, IRI 2018*, pp. 465–471, Aug. 2018, doi: 10.1109/IRI.2018.00074.

[54] P. Chudzik, S. Majumdar, F. Calivá, B. Al-Diri, and A. Hunter, "Microaneurysm detection using fully convolutional neural networks," *Comput Methods Programs Biomed*, vol. 158, pp. 185–192, May 2018, doi: 10.1016/J.CMPB.2018.02.016.

[55] Y. Yan, J. Gong, and Y. Liu, "A Novel Deep Learning Method for Red Lesions Detection Using Hybrid Feature," *Proceedings of the 31st Chinese Control and Decision Conference, CCDC 2019*, pp. 2287–2292, Jun. 2019, doi: 10.1109/CCDC.2019.8833190.

[56] K. Adem, "Exudate detection for diabetic retinopathy with circular Hough transformation and convolutional neural networks," *Expert Syst Appl*, vol. 114, pp. 289–295, Dec. 2018, doi: 10.1016/J.ESWA.2018.07.053.

[57] H. Wang *et al.*, "Hard exudate detection based on deep model learned information and multi-feature joint representation for diabetic retinopathy screening," *Comput Methods Programs Biomed*, vol. 191, p. 105398, Jul. 2020, doi: 10.1016/J.CMPB.2020.105398.

[58] P. Furtado, "Multi-class segmentation of Diabetic Retinopathy lesions: Effects of metrics, improvements and loss," *Proceedings - 19th IEEE International Conference on Machine Learning and Applications, ICMLA 2020*, pp. 1410–1417, Dec. 2020, doi: 10.1109/ICMLA51294.2020.00219.

[59] N. Shaukat, J. Amin, M. I. Sharif, M. I. Sharif, S. Kadry, and L. Sevcik, "Classification and Segmentation of Diabetic Retinopathy: A Systemic Review," *Applied Sciences 2023, Vol. 13, Page 3108*, vol. 13, no. 5, p. 3108, Feb. 2023, doi: 10.3390/APP13053108.

[60] T. Kauppi, V. Kalesnykiene, J. Kamarainen, L. L.- BMVC, and undefined 2007, "The diaretdb1 diabetic retinopathy database and evaluation protocol.," *it.lut.fi*, Accessed: May 01, 2023. [Online]. Available: https://www.it.lut.fi/project/imageret/diaretdb1/doc/diaretdb1_techreport_v_1_1.pdf

[61] T. Li, Y. Gao, K. Wang, S. Guo, H. Liu, and H. Kang, "Diagnostic assessment of deep learning algorithms for diabetic retinopathy screening," *Inf Sci (N Y)*, vol. 501, pp. 511–522, Oct. 2019, doi: 10.1016/J.INS.2019.06.011.

[62] M. Karakaya and R. E. Hacisoftaoglu, "Comparison of smartphone-based retinal imaging systems for diabetic retinopathy detection using deep learning," *BMC Bioinformatics*, vol. 21, no. 4, pp. 1–18, Jul. 2020, doi: 10.1186/S12859-020-03587-2/TABLES/3.

[63] M. A. P. Vilela, F. M. Valença, P. K. M. Barreto, C. E. V. Amaral, and L. C. Pellanda, "Agreement between retinal images obtained via smartphones and images obtained with retinal cameras or fundoscopic exams – Systematic review and meta-analysis," *Clinical Ophthalmology*, vol. 12, pp. 2581–2589, 2018, doi: 10.2147/OPTH.S182022.

[64] R. Hu, R. J. Chalakkal, G. Linde, and J. S. Dhupia, "Multi-image Stitching for Smartphone-based Retinal Fundus Stitching," *IEEE/ASME International Conference on Advanced Intelligent Mechatronics, AIM*, vol. 2022-July, pp. 179–184, 2022, doi: 10.1109/AIM52237.2022.9863260.

[65] R. Besenczi, J. Tóth, and A. Hajdu, "A review on automatic analysis techniques for color fundus photographs," *Comput Struct Biotechnol J*, vol. 14, pp. 371–384, 2016, doi: 10.1016/J.CSBJ.2016.10.001.

[66] X. Xu *et al.*, "Smartphone-Based Accurate Analysis of Retinal Vasculature towards Point-of-Care Diagnostics," *Scientific Reports 2016 6:1*, vol. 6, no. 1, pp. 1–9, Oct. 2016, doi: 10.1038/srep34603.

[67] M. Hossain, W. N. M. Isa, A. Ali, W. M. D. W. Zaki, N. Hashim, and A. Hussain, "Optimized Smartphone-based Implementation of B-COSFIRE Filter for Retinal Blood Vessel Segmentation," *2022 IEEE International Conference on Computing, ICOCO 2022*, pp. 74–79, 2022, doi: 10.1109/ICOCO56118.2022.10031761.

[68] T. T. Khaing, P. Aimmanee, S. Makhanov, and H. Haneishi, "Vessel-based hybrid optic disk segmentation applied to mobile phone camera retinal images," *Med Biol Eng Comput*, vol. 60, no. 2, pp. 421–437, Feb. 2022, doi: 10.1007/S11517-021-02484-X.

[69] R. E. Hacisoftaoglu, M. Karakaya, and A. B. Sallam, "Deep learning frameworks for diabetic retinopathy detection with smartphone-based retinal imaging systems," *Pattern Recognit Lett*, vol. 135, pp. 409–417, Jul. 2020, doi: 10.1016/J.PATREC.2020.04.009.

[70] S. Sengupta, M. D. Sindal, P. Baskaran, U. Pan, and R. Venkatesh, "Sensitivity and Specificity of Smartphone-Based Retinal Imaging for Diabetic Retinopathy: A Comparative Study," *Ophthalmol Retina*, vol. 3, no. 2, pp. 146–153, Feb. 2019, doi: 10.1016/J.ORET.2018.09.016.

[71] R. Rajalakshmi, R. Subashini, R. M. Anjana, and V. Mohan, "Automated diabetic retinopathy detection in smartphone-based fundus photography using artificial intelligence," *Eye 2018 32:6*, vol. 32, no. 6, pp. 1138–1144, Mar. 2018, doi: 10.1038/s41433-018-0064-9.

[72] O. Russakovsky *et al.*, "ImageNet Large Scale Visual Recognition Challenge," *Int J Comput Vis*, vol. 115, no. 3, pp. 211–252, Dec. 2015, doi: 10.1007/S11263-015-0816-Y.

[73] P. Iakubovskii, "Segmentation Models," *GitHub repository*. GitHub, 2019.